Anal. Chem. **2004,** *76,* 1222−1227

Articles

Concentrating Solutes and Nanoparticles within Individual Aqueous Microdroplets

Mingyan He, Chenhang Sun, and Daniel T. Chiu*

Department of Chemistry, University of Washington, Seattle, Washington 98195-1700

This paper describes a method to concentrate solutes and colloidal entities, from small ions and molecules to proteins and nanoparticles, within individual aqueous microdroplets in oil. The mechanism lies in the entrapment of the solutes within an aqueous microdroplet, while the water molecules from the droplet slowly dissolve into the organic phase. Because the rate of change in concentration scales as the fifth power of the surface-area-to-volume ratio of the droplet, this phenomenon is prominent mostly in the micrometer-length scale. This paper presents measurements that quantify the degree of solute entrapment within the microdroplet and further describes the dynamics of droplet shrinkage and the factors that influence the rate of shrinkage. In addition, this paper explains why this concentration effect does not occur for certain organic microdroplets in aqueous solutions.

Monodisperse aqueous droplets ranging from hundreds of micrometers to a few micrometers in diameter can be generated in microfluidic systems.[1,2] As discreet containers, these droplets have corresponding volumes of nanoliters (10^{-9} L) to femtoliters (10^{-15} L). We are exploring the use of these droplets as nanoscale reaction vessels for the chemical manipulations and analysis of subcellular compartments and organelles (e.g., individual mitochondria and single synaptic vesicles) at the level of single copies.[3] Aqueous microdroplets possess a number of attractive attributes as nanoreactors: (1) individual droplets can be manipulated both optically[4−6] and electrically;[7−9] (2) single subcellular compartments can be manipulated and encapsulated into a droplet with high precision and control; (3) aqueous droplets can be fused easily, so their respective contents can be combined and their reaction can be initiated;[4,5] and (4) many droplets can be manipulated, transported, and fused in parallel, which opens the potential for carrying out combinatorial operations and reactions within such droplets. Aqueous droplets represent an important area of research in down-scaled analytical techniques,[10,11] as reflected in the wide range of work in the literature on levitating droplets in air (or inert gas)[11−14] and in detecting molecules within such droplets.[13,14]

In the chemical analysis of individual subcellular organelles in which the number of molecules to be analyzed is limited,[15,16] the ability to concentrate the reactants within the reaction vessel is critical. For example, to react (e.g., fluorescent labeling) the contents of a single synaptic vesicle having a diameter of 50 nm, even if the reaction can be performed in a 1-μm diameter droplet, it would still correspond to a 8000-fold dilution as the $\sim 6 \times 10^{-20}$ L volume of the synaptic vesicle is combined with the $\sim 5 \times 10^{-16}$ L volume of the droplet. Once the biomolecules are tagged with a good fluorophore, however, sensitive single-molecule fluorescence techniques can be used to detect their presence. In such nanoscale bioanalytical applications, therefore, the key to successful analysis lies in the ability to concentrate the extremely limited amount of biological samples in ultrasmall volumes so efficient derivatization of the sample with a good fluorescent tag can occur. To address this challenge, we describe here a flexible approach to concentrate dissolved species within individual aqueous microdroplets to very high levels. This method exploits the high surface-area-to-volume ratio characteristic of microdroplets and is based on the slow dissolution of water molecules into the organic phase while the solutes are retained within the droplet.

(1) Thorsen, T.; Roberts, R. W.; Arnold, F. H.; Quake, S. R. *Phys. Rev. Lett.* **2001**, *86*, 4163−4166.
(2) Kawakatsu, T.; Tragardh, G.; Tragardh, C.; Nakajima, M.; Oda, N.; Yonemoto, T. *Colloid Surface A* **2001**, *179*, 29−37.
(3) Chiu, D. T. *Trends Anal. Chem.* **2003**, *22*, 528−536.
(4) Sasaki, K.; Koshioka, M.; Misawa, H.; Kitamura, N.; Masuhara, H. *Appl. Phys. Lett.* **1992**, *60*, 807−809.
(5) Yao, H.; Ikeda, H.; Inoue, Y.; Kitamura, N. *Anal. Chem.* **1996**, *68*, 4304−4307.
(6) Kuyper, C. L.; Chiu, D. T. *Appl. Spectrosc.* **2002**, *56*, 300A−312A.
(7) Kuo, J. S.; Spicar-Mihalic, P.; Rodriguez, I.; Chiu, D. T. *Langmuir* **2003**, *19*, 250−255.
(8) Cho, S. K.; Moon, H. J.; Kim, C. J. *J. Microelectromech. S.* **2003**, *12*, 70−80.
(9) Ren, H.; Fair, R. B.; Pollack, M. G.; Shaughnessy, E. J. *Sens. Actuators, B* **2002**, *87*, 201−206.
(10) Yi, C.; Huang, D.; Gratzl, M. *Anal. Chem.* **1996**, *68*, 1580−1584.
(11) Petersson, M.; Nilsson, J.; Wallman, L.; Laurell, T.; Johansson, J.; Nilsson, S. *J. Chrom., B* **1998**, *714*, 39−46.
(12) Welter, E.; Neidhart, B. *Fresenius' J. Anal. Chem.* **1997**, *357*, 345−350.
(13) Santesson, S.; Andersson, M.; Degerman, E.; Johansson, T.; Nilsson, J.; Nilsson, S. *Anal. Chem.* **2000**, *72*, 3412−3418.
(14) Barnes, M. D.; Ng, K. C.; Whitten, W. B.; Ramsey, J. M. *Anal. Chem.* **1993**, *65*, 2360−2365.
(15) Chiu, D. T.; Lillard, S. J.; Scheller, R. H.; Zare, R. N.; Rodriguez-Cruz, S. E.; Williams, E. R.; Orwar, O.; Sandberg, M.; Lundqvist, J. A. *Science* **1998**, *279*, 1190−1193.
(16) Chiu, D. T.; Wilson, C. F.; Ryttsen, F.; Stromberg, A.; Farre, C.; Karlsson, A.; Nordholm, S.; Gaggar, A.; Modi, B. P.; Moscho, A.; Garza-Lopez, R. A.; Orwar, O.; Zare, R. N. *Science* **1999**, *283*, 1892−1895.

10.1021/ac035196a CCC: $27.50
Published on Web 02/04/2004

Table 1. Tabulation of the Shrinkage Behavior of Aqueous Microdroplets under Different Experimental Conditions

method of droplet generation	presence of solute/nanoparticle	organic continuous phase	substrate	shrinkage rate dA/dt (μm^2/min)	residue left
in Petri dish	none	soybean oil	none	258	no
in Petri dish	sodium chloride	soybean oil	none	298	yes
in Petri dish	carbonic anhydrase	soybean oil	none	254	yes
in Petri dish	27-nm nanoparticle	soybean oil	none	364	yes
in Petri dish	Alexa	soybean oil	polystyrene	148	yes
in Petri dish	none	soybean oil	polystyrene	126	no
in microchannel	none	soybean oil	PDMS	402	no
in Petri dish	none	light mineral oil	polystyrene	17	no
in Petri dish	none	*n*-hexadecane	polystyrene	5.3	no

EXPERIMENTAL SECTION

Fabrication of Microchannels and in-Channel Generation of Microdroplets. Microchannels were fabricated in poly(dimethylsiloxane) (PDMS), and the fabrication procedure has been described in detail elsewhere.[17−21] Treatment of the PDMS surface in an oxygen plasma was used both to seal together irreversibly the two surfaces that were brought into contact to form an enclosed microchannel and to render the surfaces hydrophilic. To create microchannels with hydrophobic surfaces, the sealed PDMS channel system was placed in an oven and heated to 120 °C for at least 2 h. The height of the microchannels in our experiments was 15 μm, which was determined by the thickness of the spin-coated negative photoresist (SU-8). The width of the orifice through which microdroplets were generated was 16 μm. Organic droplets in water were generated at the T-junction of the hydrophilic channel on the basis of the shear-force method,[1,22] whereas water droplets in oil were created at the orifice of a hydrophobic microchannel as the aqueous phase entered a chamber filled with oil. If the diameter of the droplet is bigger than the height of the microchannel, the droplet is sandwiched between the floor and ceiling of the channel.

Generation of Aqueous Microdroplets in Petri Dish. This method in generating aqueous microdroplets was faster and easier than in-channel droplet generation, but it provides little control over the sizes of droplets that were formed. A small Petri dish was filled with oil (∼15 mL), and a small drop of water (10 μL) was injected into the oil from a micropipet. A plastic pipet was used to stir and break up the drop of water until small droplets with diameters in the range of 1−500 μm were formed. If air bubbles were created during the process, they usually floated to the top surface of the oil and could be removed by suction into the pipet. Because the density of aqueous droplets (e.g., 1.0 g/cm^3 for water) is slightly greater than that of the oils we used (e.g., 0.92 g/cm^3 for soybean oil), the aqueous droplets tend to sediment slowly to the bottom of the Petri dish. The free-floating droplets we measured in this paper, however, did not reach the bottom of the dish during our period of observation (<70 min).

Visual Observation of Individual Microdroplets. The droplets were observed at room temperature with an upright microscope (Leitz, Wetzlar, Germany) using a long working distance 20× objective. A high-sensitivity camera (Cohu 4910, San Diego, CA) was used to monitor changes in the size of droplets as well as for fluorescence imaging. For bright-field imaging, the intensity of the illumination light was set at a very low level to avoid heating the objects that were being visualized. For fluorescence imaging, an excitation filter was used to isolate the blue emission from a Xenon Arc lamp for illumination. To minimize photobleaching of dyes, the blue excitation light was allowed to illuminate the sample for only a couple of seconds during data acquisition.

Materials and Chemicals. For aqueous droplets in oil, the disperse phase was pure deionized (DI) water or DI water containing one of the following solutes or nanoparticles: sodium chloride (Fisher, Fair Lawn, NJ), Alexa 488 hydrazide sodium salt (Molecular Probes, Eugene, OR), carbonic anhydrase (CA) from Sigma (St. Louis, MO) labeled with fluorescein-5-isothiocyanate (FITC) from Molecular Probes (Eugene, OR), or 27-nm yellow-green fluorescent carboxylate-modified polystyrene sphere (Molecular Probes, Eugene, OR). To dye-tag CA with FITC, we prepared 10 mg/mL CA solution in 0.1 M $NaHCO_3$ (Sigma, St. Louis, MO) and 10 mg/mL FITC dye in DMSO (Fisher, Fair Lawn, NJ) solution. We then mixed 1 mL of the CA solution with 100-μL of the FITC solution, and incubated the reaction for 1 h at room temperature with continuous stirring. The labeled CA was purified from unreacted FITC by running the reaction mixture through a size-exclusion column (Bio-Rad, Econo-Pac 10 DG, Hercules, CA). The continuous phase for aqueous droplets was soybean oil (Ventura Foods, City of Industry, CA), light mineral oil (Fisher, Fair Lawn, NJ), or *n*-hexadecane (Sigma, St. Louis, MO).

RESULTS AND DISCUSSIONS

Shrinkage of Individual Aqueous Microdroplets. Table 1 summarizes our observation of the shrinkage of aqueous microdroplets under different experimental conditions. Figure 1A−D shows deionized (DI) water droplets in soybean oil that were generated as the aqueous phase passed through an orifice and entered into a chamber that was filled with the oil. These droplets, with a diameter of 10−30 μm, shrank and dissolved into the continuous phase over a period of ∼5 min at a rate of ∼402 μm^2/min (changes in the surface area over time). Similar behavior was observed for free-floating DI water droplets that were produced outside of microchannels in an oil bath in a Petri dish, but at a

(17) Shelby, J. P.; Chiu, D. T. *Anal. Chem.* **2003**, *75*, 1387−1392.
(18) Allen, P. B.; Rodriguez, I.; Kuyper, C. L.; Lorenz, R. M.; Spicar-Mihalic, P.; Kuo, J. S.; Chiu, D. T. *Anal. Chem.* **2003**, *75*, 1578−1583.
(19) McDonald, J. C.; Duffy, D. C.; Anderson, J. R.; Chiu, D. T.; Wu, H. K.; Schueller, O. J. A.; Whitesides, G. M. *Electrophoresis* **2000**, *21*, 27−40.
(20) Xia, Y. N.; Whitesides, G. M. *Angew. Chem., Int. Ed.* **1998**, *37*, 551−575.
(21) Anderson, J. R.; Chiu, D. T.; Jackman, R. J.; Cherniavskaya, O.; McDonald, J. C.; Wu, H. K.; Whitesides, S. H.; Whitesides, G. M. *Anal. Chem.* **2000**, *72*, 3158−3164.
(22) Song, H.; Tice, J. D.; Ismagilov, R. F. *Angew. Chem., Int. Ed.* **2003**, *42*, 768−772.

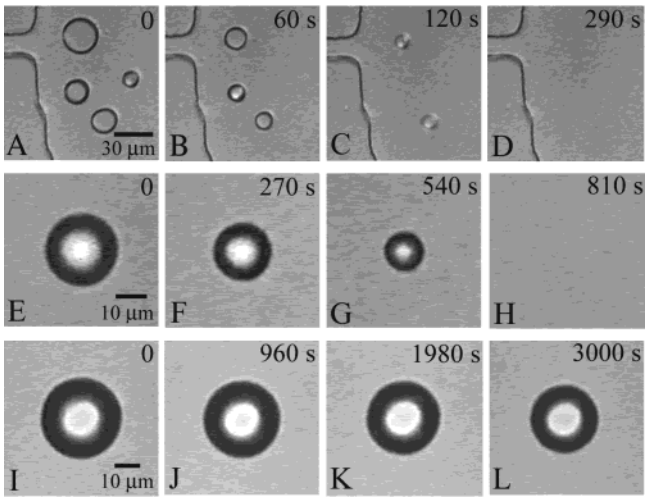

Figure 1. Sequence of micrographs showing the shrinkage of DI water droplets over time under three different conditions. (A−D) DI water droplets in soybean oil in contact with the hydrophobic surface of a PDMS microfluidic system. (E−H) DI water droplet in soybean oil in contact with the surface of the polystyrene Petri dish. (I−L) DI water droplet in light mineral oil in contact with the polystyrene surface.

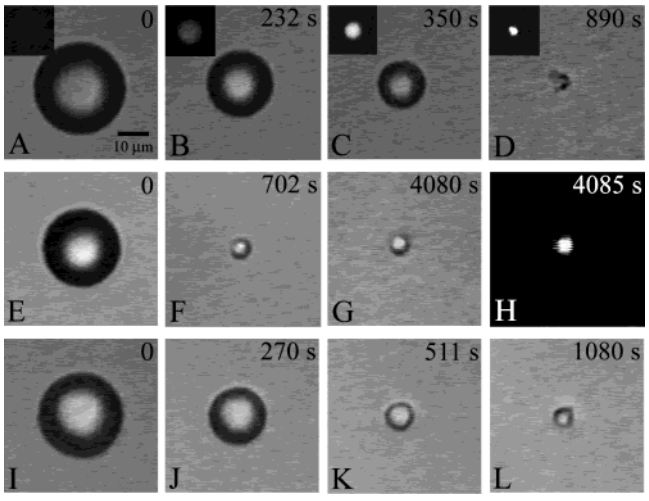

Figure 2. Sequence of micrographs showing the concentration of different types of nanoparticles and solutes within free-floating aqueous microdroplets in soybean oil. (A−D) Fluorescent polystyrene nanoparticles (27 nm in diameter) were concentrated inside an aqueous droplet; the insets are the corresponding fluorescence images showing increases in fluorescence intensity as the concentration of beads increased. (E−H) Shrinkage of an aqueous droplet containing dye-labeled carbonic andydrase; the microdroplet shrank gradually over the first ∼12 min (E−F), after which the size of the droplet remained fairly constant (F−G). (H) shows the fluorescence image of the concentrated dye-tagged protein. (I−L) Concentration of sodium chloride in an aqueous droplet. The droplet shrank over the first ∼9 min (I−K), after which the shape and size of the droplet remained fairly constant for the remaining 18 min (L). The scale bar applies to all panels (A−L).

slower rate of shrinkage (∼258 μm^2/min). Figure 1E−H shows the shrinkage and complete dissolution in soybean oil of a DI water droplet with a diameter of 23 μm in contact with polystyrene over a period of 13.5 min at a rate of 126 μm^2/min. Dissolution of the droplets was observed both for those that were in contact with a hydrophobic substrate (e.g., polystyrene and PDMS) and for those that freely floated in the continuous phase (see Table 1). Droplets that were in contact with substrates generally have a slower rate of shrinkage, with the exception of those inside microchannels. Figure 1I−L shows that the rate of droplet shrinkage is dramatically reduced in light mineral oil (17 μm^2/min), whereas in *n*-hexadecane, the rate was even slower at 5.3 μm^2/min. In later sections, we will describe in detail the factors that influence the rate of droplet shrinkage.

Concentration of Solutes Within Aqueous Microdroplets. We explored the possibility of exploiting this slow dissolution of water molecules into the organic phase as a platform for concentrating analytes entrapped within a microdroplet. Because most biological molecules of interest (e.g., proteins, peptides, metabolites, amino acids, and ions) contain charges and polar groups, their partition coefficients in most organic phases are negligible. Thus, these biological molecules cannot dissolve into oil as the water molecules exit the microdroplet. Figure 2 shows the concentration of nanoparticles, proteins, and salts within individual water droplets dispersed in soybean oil. The droplet in Figure 2A−D contained 27-nm fluorescent polystyrene beads, which became concentrated as the droplet shrank. The insets are the corresponding fluorescence images showing the expected increase in fluorescence intensity. Figure 2D shows the resulting aggregate of beads after dissolution of the water molecules from the microdroplet. Figure 2E−H shows the concentration of proteins within a microdroplet, in which fluorescein-labeled carbonic anhydrase was dissolved. This droplet shrank gradually over 700 s or ∼12 min (Figure 2E to F), after which the size of the droplet remained constant over our period of observation for the next ∼56 min (Figure 2F to G). Figure 2H shows the resultant fluorescence image. Figure 2I−L shows a droplet that contained sodium chloride. The size of the droplet decreased gradually, and the shape of the droplet remained spherical for the first 511 s or ∼8.5 min (Figure 2I to K). The droplet then experienced a period (∼1 min) of rapid nonspherical deformation, after which its size and shape remained constant as represented by Figure 2L.

For DI water droplets that did not contain any solutes, the droplet continued to shrink until it was completely dissolved into the organic phase (Figure 1). For droplets that did contain solutes (Figure 2), we have always observed the formation of residues, in which case the size of the droplet initially decreased with time until it had reached its final size (Figure 2F to G and 2K to L). Such residues can be spherical (Figure 2G) or nonspherical (Figure 2D) depending on the dissolved solutes. Even if the final shape of the residue was spherical, deformation of the droplet was often observed during the last stage of shrinkage. For example, there was nonspherical deformation of the droplet right before the formation of the spherical residue shown in Figure 2F. Unlike solid-phase extraction, this method concentrates *all* encapsulated solutes within the droplet rather than a particular solute selectively.

Quantitative Measurements of Solute Entrapment. To quantify this concentration effect, Figure 3 plots the increase in fluorescence intensity as the water droplet containing a fluorescent dye, Alexa-488, decreases in volume in a continuous phase of soybean oil. For an ideal nonsaturated and nonphotobleachable dye and provided the depth of focus of the objective lens (∼6 μm in our case) is smaller than the diameter of the droplet, the observed fluorescence intensity should be proportional to the

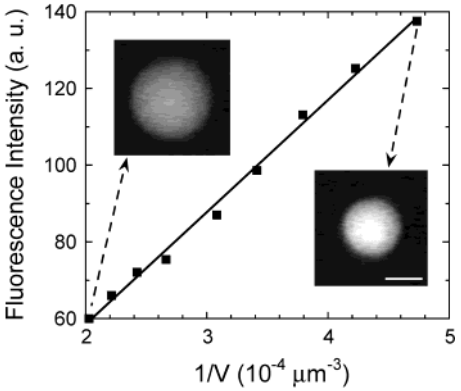

Figure 3. A plot showing the measured fluorescence intensity of an aqueous droplet, which contained the fluorescent dye Alexa-488, increased linearly with the reciprocal of the volume of the droplet. The solid line is a linear fit. The insets show the corresponding fluorescence images of the droplet at the indicated time points. The scale bar represents 10 μm and applies to both insets.

concentration of the dye (C_s) in the droplet,

$$F \propto C_s \propto \frac{1}{V} = \frac{3}{4\pi r^3} \tag{1}$$

where F is the fluorescence intensity, and V and r are the volume and the radius of the droplet, respectively. The fluorescence intensity was obtained from a spatial average of the digitized gray-value measurements, in which the intensity from the inner two-thirds of the droplet was used to avoid any blurring effects caused by the boundary of the droplet. The fluorescence intensity we used was calculated by subtracting the background noise (G_0) from the measured average gray-value intensity (G).

Figure 3 shows a linear fit between the observed increase in the fluorescence intensity versus the corresponding decrease in droplet volume. The ~2.3 times increase in the fluorescence intensity matches perfectly the ~2.3 times decrease in volume, which indicates that Alexa was concentrated gradually inside the aqueous droplet and did not diffuse into the organic phase, as anticipated. As the droplet continued to shrink, however, we did observe a maximum and then a gradual decrease in the observed fluorescence intensity. The observed intensity plateaus because as the diameter of the droplet becomes smaller than the depth of focus, eq 1 is no longer valid, since the number of fluorescent molecules within the probe volume does not change with increases in concentration. The eventual decrease in fluorescence intensity suggests Alexa may self-quench at high concentrations. The key point here, however, is that Alexa molecules (and presumably other charged molecules, such as amino acids and proteins) were fully retained in the droplet and could be quantitatively concentrated as the droplet shrank.

Dynamics of Shrinkage of Aqueous Microdroplets. Figure 4A shows that the surface area of a pure water droplet in soybean oil decreased linearly with the increase of time. However, for a water droplet that contained sodium chloride (Figure 4B), two regimes in the droplet shrinkage were observed. In regime I, the surface area of the droplet decreased linearly with the increase of time, with nonlinear deviation around the end of this regime. In regime II, the surface area of the "droplet" or residue remained

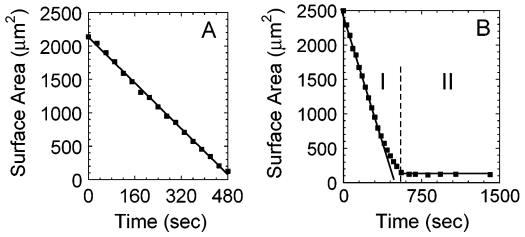

Figure 4. (A) The surface area of a free-floating DI water droplet in soybean oil decreased linearly with time. (B) The shrinkage of water droplet containing sodium chloride in soybean oil can be divided into two time regimes. In regime I, the surface area of the droplet decreased linearly with time, with nonlinear deviations close to the end of this region. In regime II, the size of droplet/residue remained constant. Solid lines are linear fits.

constant. We defined "shrinkage rate" as the slope in regime I. For aqueous droplets that contained dye-labeled proteins or fluorescent molecules, the relationship between surface area and time is similar to the one shown in Figure 4B, except that the shrinkage rates and nonlinear deviations vary. For aqueous droplets containing nanoparticles, however, no nonlinear deviation was observed at the end of regime I. In the following, we present a model that describes the dynamics of droplet shrinkage.

For a pure water droplet in oil (suppose oil is stagnant), the diffusion rate (N_w, in unit of mol s^{-1} m^{-2}) of water molecules from the droplet to the surrounding oil is[23]

$$N_w = \frac{D_{wo}}{r}(C_w - C_{w-ref}) \tag{2}$$

where D_{wo} is the diffusivity of water in oil, and C_w and C_{w-ref} are the concentrations of water on the surface of the droplet and at a reference point far away from the droplet, respectively.

The diffusion rate can be rewritten as

$$N_w = -\frac{d(m_w/M_w)}{A\,dt} = -\frac{\rho_w}{M_w A}\frac{dV}{dt} = -\frac{\rho_w}{M_w}\frac{dr}{dt} \tag{3}$$

where m_w is the mass of water in the aqueous droplet; M_w and ρ_w are the molecular weight and density of water, respectively; A is the surface area of the droplet; and t is time.

Suppose C_{w-ref} does not change with time (e.g., at steady state), from eq 2 and 3, we get

$$\frac{dr}{dt} = -\frac{M_w D_{wo}(C_w - C_{w-ref})}{\rho_w r}$$
$$\frac{dA}{dt} = -\frac{8\pi M_w D_{wo}(C_w - C_{w-ref})}{\rho_w} = -k_1$$
$$A = -k_1 t + k_2 \tag{4}$$

where k_1 and k_2 are constants. k_1 is what we called the "shrinkage rate". Equation 4 shows that the surface area of the water droplet

(23) Geankoplis, C. J. *Transport Processes and Unit Operations*; Prentice Hall PTR: Engelwood Cliffs, NJ, 1993.

in oil decreases linearly with the increase of time, which is similar to the evaporation of water drops in stagnant dry air.[24,25]

From our experimental results, eq 4 is valid for a free-floating water droplet with Brownian motion and sedimentation (Figure 4A). In addition, eq 4 can be considered to be valid for an aqueous droplet with dilute solutes (Figure 4B, regime I). However, nonlinear deviations can be expected for a concentrated droplet, as shown in Figure 4B close to the end of regime I. Such deviations are caused by the changes of relative concentration of water at the droplet surface.

Because the surface-to-volume ratio (SV) scales as $1/r$ with the radius of a spherical droplet, the rate of change in solute concentration (dC_s/dt) as a function of surface-to-volume ratio for an aqueous droplet containing dilute solute is

$$\frac{dC_s}{dt} \propto \frac{1}{r^4}\frac{dr}{dt} \propto \frac{1}{r^5} \propto (SV)^5 \qquad (5)$$

whereas the rate of change of surface-to-volume ratio ($d(SV)/dt$) versus the radius of the droplet is $1/r^3$.

Equation 5 indicates that the rate of change in concentration of the solute inside a dilute aqueous droplet scales as the fifth power of its surface-to-volume ratio. Because of this strong dependence on the surface-to-volume ratio of the droplet, the concentration effect cannot be readily observed within short time scales at the macroscale where surface-to-volume ratio is low. In the micro- and nanometer length scale, however, this effect becomes noticeable and practical to implement. The size range of the droplets studied here (from tens of micrometers to a few micrometers) is comparable to or slightly larger than the size of a typical mammalian cell, which makes this range of droplet sizes suitable for applications in single-cell and subcellular analysis.

Influence of the Organic Phase on Shrinkage of Aqueous Droplets. One important factor that affects droplet shrinkage lies in the organic phase, as would be expected on the basis of the differences in the solubility of water in different types of oil or organic solvents. Soybean oil is composed of triacylglycerols derived from glycerol and carboxylic acids, of which the main components are linoleic acid (50−60%), oleic acid (22−34%), and palmitic acid (7−11%). Because of the presence of the ester groups, a small amount (0.3 volume % as we calculated in later sections) of water can be dissolved into soybean oil (Figure 1A−H). In contrast, light mineral oil is a mixture of hydrocarbons mainly composed of alkanes in the range of 15−50 carbons, which makes the dissolution of water molecules into it highly unfavorable (Figure 1I−L). The slowness of droplet evaporation in a suitable organic phase (over minutes) may prove to be an important advantage because it offers more precise control over the evaporation process. By tuning the composition of the organic phase and by placing individual droplets in different organic environments created within microfluidic systems, the rate and extent of the droplet shrinkage can be exquisitely controlled.

Effects of Concentration Gradients on the Rate of Droplet Shrinkage. We have made two observations on the rate of droplet shrinkage (Table 1): (1) outside of microchannels, a free-floating droplet generally shrinks faster than a droplet in contact with a substrate; and (2) inside microchannels, a droplet usually shrinks at a significantly faster rate in comparison with that outside of channels. For example, the shrinkage rate of a freely floating DI water droplet was 258 $\mu m^2/min$, whereas inside microchannels, despite the droplets' being in contact with a hydrophobic substrate, the rate of shrinkage was 402 $\mu m^2/min$.

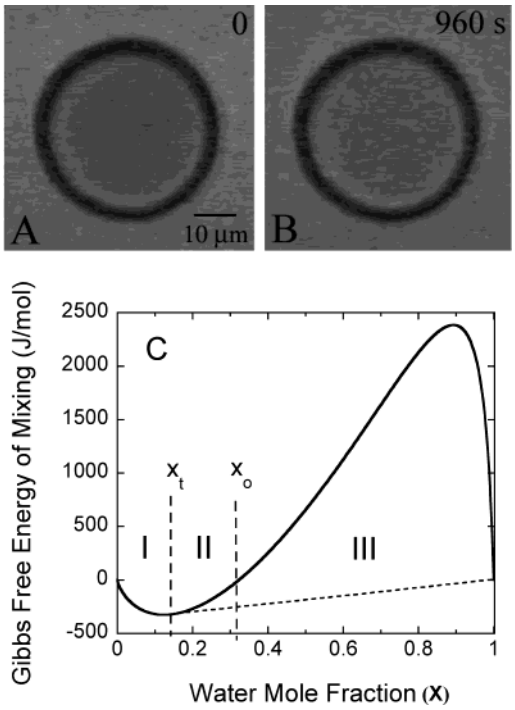

Figure 5. (A−B) Images showing the size of the soybean oil droplet in DI water remained constant over our period of observation (16 min). (C) The Gibbs free energy of mixing of soybean oil and water at 25 °C as a function of the water mole fraction, x, as calculated by UNIFAC. x_t is associated with the tangent point on the curve, and x_0 is the water mole fraction above which the Gibbs free energy of mixing becomes positive. The water−oil solution is stable in regime I, metastable in regime II, and unstable in regime III in which phase splitting is guaranteed.

These differences in the rates of shrinkage were caused by the differences in the concentration gradients of water surrounding the droplet. If the concentration of water reaches the maximum saturation level in the bulk oil, there is no concentration gradient, and the rate of droplet shrinkage would be 0. In our experiment, the water−oil volume ratio is ~0.07%, which is much smaller than the saturation concentration for water in soybean oil of 0.3%.

For an aqueous droplet in contact with a hydrophobic substrate, the surrounding oil does not move. In contrast, for a free-floating droplet, which undergoes Brownian motion and sedimentation, the surrounding oil is less saturated with water because it is frequently replaced. Thus, C_{w-ref} (with the same distance between the droplet and the reference point) of a free-floating droplet is smaller in eq 4 than for an immobile droplet. Therefore, a droplet in contact with a surface would have a smaller rate of dissolution. Despite the presence of surface contacts, an aqueous droplet localized inside a microchannel has a much faster rate of shrinkage over those dispersed in bulk fluid. This discrepancy can be explained by the presence of siphoning in microchannels, which leads to oil flow and, thus, efficient mass transfer of water away from the droplet and into oil.

(24) Ranz, W. E.; Marshall, W. R. *Chem. Eng. Prog.* **1952**, *48*, 173−180.
(25) Ranz, W. E.; Marshall, W. R. *Chem. Eng. Prog.* **1952**, *48*, 141−146.

Behavior of Organic Microdroplets in Water. In contrast to aqueous droplets in soybean oil, we did not observe noticeable shrinkage of a droplet of soybean oil in water (Figure 5). This asymmetric behavior suggests that although a finite amount of water can dissolve in soybean oil, the vice versa is thermodynamically unfavorable. To explain this asymmetry, we have calculated the Gibbs free energy of mixing (g^{mix}) on a per mole basis for water and soybean oil using the universal functional activity coefficient (UNIFAC) method.[26] In UNIFAC, solutions are treated as mixtures not of molecules, but of functional groups, out of which the original molecules can be reconstructed. The relative volumes, areas, and interaction parameters of 64 main groups and twice as many subgroups have been published.[27] UNIFAC directly yields the excess activity coefficients of the compounds in the solution, which are then used to calculate the excess Gibbs free energy of mixing. The actual Gibbs free energy of mixing, g^{mix}, was obtained by adding this excess Gibbs free energy of mixing to the ideal Gibbs free energy of mixing. A combination of triacylglycerols with 60% linoleic acid, 30% oleic acid, and 10% palmitic acid was used in our UNIFAC calculation to model soybean oil.

Figure 5C plots the g^{mix} of water and soybean oil at 25 °C versus the mole fraction of water. Because the miscibility of two liquids requires both

$$g^{mix} < 0 \quad \text{and} \quad \left(\frac{\partial^2 g^{mix}}{\partial x^2}\right)_{T,P} > 0 \qquad (6)$$

where T is temperature and P is pressure, a solution of water and soybean oil is stable in regime I ($x < x_t$), metastable in regime II ($x_t < x < x_o$), and unstable in regime III ($x > x_o$). To minimize the total free energy of the system, phase splitting into a pure water phase and a water−oil solution that has a water mole fraction of x_t is very likely in regime II and is guaranteed in regime III. From this plot, water can dissolve in soybean oil up to 14 mol % (x_t) or 0.3 volume % while soybean oil cannot dissolve in water, which agrees with our experimental observations.

CONCLUSION

The concentration of molecules, which dictates their frequency of interaction, is central to chemical and biological processes. This work exploits the high surface-area-to-volume ratio characteristic of the microscale and demonstrates a flexible method to concentrate dissolved solutes and nanoparticles in aqueous microdroplets. By understanding the kintetics and the factors that affect droplet shrinkage, it should be possible to control precisely and dynamically the concentrations of dissolved species within individual droplets. In using droplets as nanoreactors for the chemical transformations of ultrasmall biological samples, this ability to concentrate the reactants will be especially critical, because such samples are often present in minute amounts. This concentrating effect will only work for solutes that do not dissolve in or react with the organic phase, which we believe is the case for many biological molecules, such as amino acids, DNA, and many proteins and metabolites. We anticipate this control over the precise concentrations of dissolved solutes within individual microdroplets to be broadly useful for studying molecular phenomena that are sensitive to concentrations, such as spatially confined chemical reactions, macromolecular crowding, and crystal formation.

ACKNOWLEDGMENT

The authors would like to thank Gina Fiorini for help with protein labeling. Support for this work from the NIH is gratefully acknowledged.

Received for review October 9, 2003. Accepted December 29, 2003.

AC035196A

(26) Fredenslund, A.; Gmehling, J.; Rasmussen, P. *Vapor-Liquid Equilibria Using UNIFAC: a Group Contribution Method*; Elsevier: New York, 1977.

(27) Wittig, R.; Lohmann, J.; Gmehling, J. *Ind. Eng. Chem. Res.* **2003**, *42*, 183−188.